Row-Action Inversion of the Barrick–Weber Equations

J. J. GREEN AND L. R. WYATT

Department of Applied Mathematics, University of Sheffield, Sheffield, United Kingdom

(Manuscript received 27 May 2004, in final form 14 April 2005)

ABSTRACT

The Barrick–Weber equations describe the interaction of radar signals with the dynamic ocean surface, and so provide a mathematical basis for oceanic remote sensing. This report considers the inversion of these equations with several of the row-action methods commonly used to solve large linear systems with unstructured sparsity. It is found that the performance of the methods in inverting both synthetic and measured Doppler spectral data is comparable, with the method of Chahine–Twomey–Wyatt offering a slight advantage in the reliability of the recovery of the full directional wave spectrum and of parameters derived from its integration. Some remarks and open questions on the ill-posedness of the inversion problem conclude the paper.

1. Introduction

The Doppler spectrum of a high-frequency (HF) radar signal backscattered from the ocean's surface contains a wealth of information on the sea state, and so naturally has attracted interest from the remote sensing community. As was shown in Weber and Barrick (1977) and Barrick and Weber (1977), the interaction of the radar with the sea's surface admits a perturbation analysis on the Doppler spectrum σ:

$$\sigma = \sigma_1 + \sigma_2 + \cdots.$$

The first term of this analysis is found to be a linear combination of Dirac delta functions δ:

$$\sigma_1(\omega, \phi) = 2^6 \pi k_0^4 \sum_{m=\pm 1} S(-m\mathbf{k}_0)\delta(\omega - m\omega_b), \quad (1)$$

where ω is the angular frequency of the Doppler shift, $\mathbf{k}_0$ is the wave vector of the incident radar signal with wavenumber k_0 and direction ϕ, S is the ocean wavenumber spectrum, and ω_b is the frequency of the Bragg-matched waves,

$$\omega_b = \sqrt{2gk_0},$$

where g is the acceleration due to gravity.

Equation (1) predicts impulses in the Doppler spectrum of the backscatter at shift frequencies $\pm\omega_b$, features that are evident in the measured spectrum, such as is illustrated in Fig. 1.

The second order of the perturbation analysis leads to the nonlinear integral equation

$$\sigma_2(\omega, \phi) = 2^6 \pi k_0^4 \sum_{m,m'=\pm 1} \int_{\mathbf{R}^2} |\Gamma|^2 S(m\mathbf{k}) S(m'\mathbf{k}') \times \delta\left(\omega - m\sqrt{gk} - m'\sqrt{gk'}\right) d\mathbf{p}, \quad (2)$$

where the wave vectors $\mathbf{k}$ and $\mathbf{k}'$ satisfy the Bragg resonance condition $\mathbf{k} + \mathbf{k}' = -2\mathbf{k}_0$, and are related to $\mathbf{p}$, the variable of integration, by

$$\mathbf{k} + \mathbf{k}_0 = \mathbf{p}, \quad \mathbf{k}' + \mathbf{k}_0 = -\mathbf{p},$$

as illustrated in Fig. 2.

The kernel of (2) is determined by the coupling coefficient $\Gamma = \Gamma(\omega, k, \theta, mm')$ accounting for nonlinear hydrodynamic and electromagnetic effects, and is described in detail in the articles by Weber and Barrick (1977), Barrick and Weber (1977), and Barrick and Lipa (1986).

The Barrick–Weber equations are amenable to linearization because the signal is dominated by the interaction between long and short ocean waves and the latter can be approximated using wind-wave models (see, e.g., Wyatt 1986; Lipa and Barrick 1986). In Green (2003), it is observed that the linearized equation may be viewed, locally, as a weighted projection transform. This leads to a method for discretization of the linear-

Corresponding author address: J. J. Green, Dept. of Applied Mathematics, University of Sheffield, Hicks Bldg., Hounsfield Rd., Sheffield S3 7RH, United Kingdom.
E-mail: j.j.green@shef.ac.uk

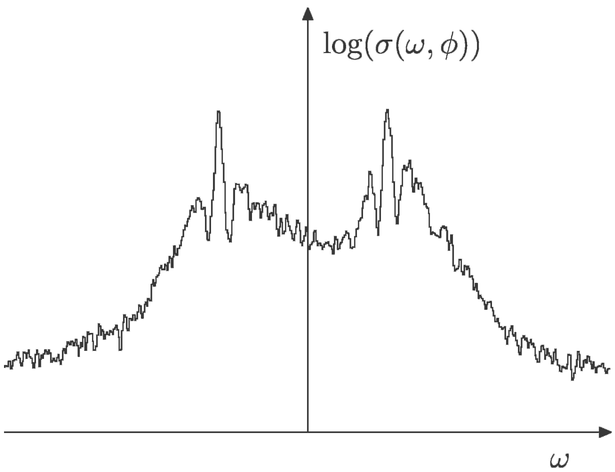

FIG. 1. An example of measured Doppler spectra.

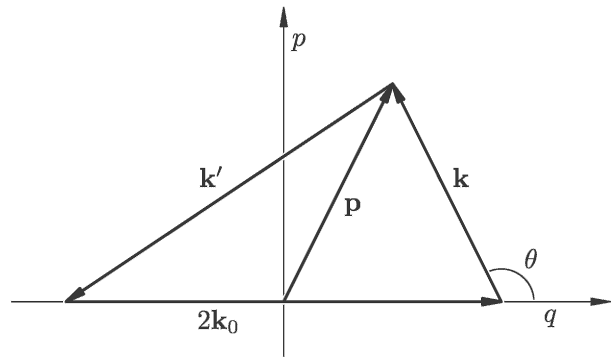

FIG. 2. Geometry of the wave vectors at second order.

ized equations based on the techniques for that of the general unweighted projection transform, that is, the discretization of transmission tomography problems. The discretization reduces the inversion of the linearized Barrick–Weber equations to the solution of a linear system:

$$\boldsymbol{\sigma} = \mathbf{A}\boldsymbol{\xi}, \tag{3}$$

where the vector $\boldsymbol{\sigma}$ represents the normalized measured Doppler spectral values (typically from more than one radar), $\boldsymbol{\xi}$ contains the coefficients of the normalized ocean wave spectrum representation, and $\mathbf{A}$ is the discretization matrix. The matrix $\mathbf{A}$ is large (in practice around 200 rows and 2000 columns) but possesses an unstructured sparsity that can be exploited to obtain rapid solutions to (3), and so to the problem of estimating the ocean wave directional spectrum from HF backscatter measurements.

In this paper we investigate the use of row-action methods in the solution of the discretization (3). We will compare synthetic wave spectra with those inverted from the deduced backscatter, and compare several ocean parameters as obtained from the inversion of measured backscatter with those obtained from a collocated buoy. In addition to comparing three row-action inversion methods, we seek to optimize a number of parameters controlling these inversions, for the purpose of calibration for forthcoming deployments.

2. Background

In this section we describe the inversion method used for the linearized Barrick–Weber equations. We begin with as full a summary of the functional representation and discretization as is required to introduce our notation; a more detailed account can be found in Green (2003).

a. Functional representation

Following Weber and Barrick (1977) and Barrick and Weber (1977), we consider the normalized directional wave spectrum $Z = S/(2k_0)^4$, and seek a representation of Z as a linear combination of basis functions b_i:

$$Z(\mathbf{y}) = \sum_i \xi_i b_i(\mathbf{y}), \tag{4}$$

where $\mathbf{y}$ is the vector in the direction of $\mathbf{k}$, but with a magnitude $y = \sqrt{k/2k_0}$ [a transformation chosen so that a uniform discretization of $\mathbf{y}$ scales approximately with the data; see Green (2003, section 3) for details]. For the basis functions b_i, we take translates of a single function Ψ, radially symmetric with respect to the Euclidean norm,

$$b_i(\mathbf{y}) = \Psi(\mathbf{y} - \mathbf{y}_i) = \psi(\|\mathbf{y} - \mathbf{y}_i\|). \tag{5}$$

The function's window, ψ, is the Lewitt–Kaiser–Bessel function (see Lewitt 1990):

$$\psi(r) = \begin{cases} (1 - (r/a)^2)^{m/2} I_m\left(\alpha\sqrt{1 - (r/a)^2}\right)/I_m(\alpha) & (r < a) \\ 0 & \text{otherwise} \end{cases}, \tag{6}$$

where I_m is the modified Bessel function of order m, as in Watson (1944). In (6), a is the radius of support of ψ, α controls the localization of ψ about the origin, and m determines the smoothness of ψ at $r = a$ and the rate of decay of its Fourier transform.

Functional representation in the form (5) was intro-

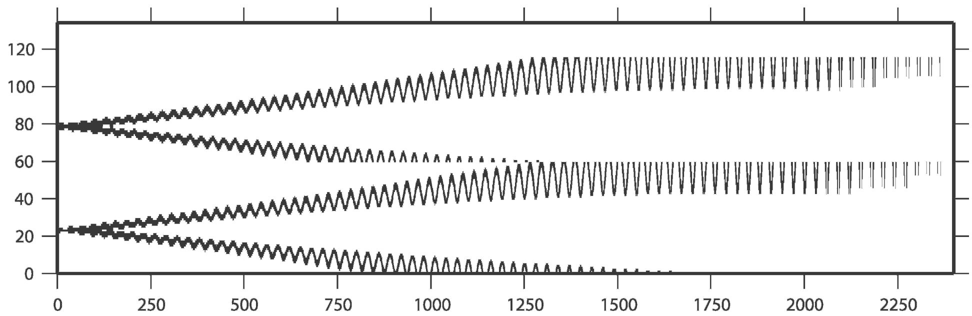

FIG. 3. Sparsity of **A**; nonzero entries shown black.

duced by Lewitt (1990) in the context of transmission tomography, that is, in the inversion of the x-ray transform. Such a representation has a number of advantages over the usual pixel-based representation. In particular,

- the smoothness of the basis function, and so of the representation, can be controlled by the adjustment of the parameter m, a fact that is important if the inversion problem is ill-posed;
- the function Ψ is computationally attractive since most interesting quantities associated with it—the Fourier transform, gradient, projection, or Abel transform—can be calculated explicitly as a result of the recurrence relations enjoyed by the Bessel function (see Lewitt 1990); and
- the choice of parameters a, m, and α can be made so as to give the representation beneficial approximation properties (Lewitt 1990; Green 2002).

In our implementation of the representation, the centers $\mathbf{y}_i$ are placed on a uniform grid in the $\mathbf{y}$ domain, that is, on the cylinder. Following the deliberations in Green (2002) we initially choose $m = 2$, $a/g = 1.78$, and $\alpha = 9.2$, where g is the grid spacing: the distance between adjacent centers $\mathbf{y}_i$.

b. Discretization

The discretization of the linearized Barrick–Weber equations with the Lewitt–Kaiser–Bessel representation (4) is straightforward. Each Doppler spectral datum,

$$\sigma_j = \frac{1}{\Delta\eta}\int_{\eta_j}^{\eta_{j+1}} \sigma(\eta)\,d\eta$$

(where $\Delta\eta$ is the sample width of the normalized Doppler shift $\eta = \omega/\omega_b$), corresponds to a strip integral over the normalized directional spectrum $Z = (2k_0)^4 S$, and making a suitable approximation we find that

$$\sigma_j = \frac{1}{\Delta\eta}\sum_i \Lambda_i B_{i,j}\xi_i,$$

where Λ is an expression accounting for the kernel of the Barrick–Weber equations, a linearization term and Jacobians of domain transformations [see Green 2003, Eq. (2.6)], $\Lambda_i = \Lambda(\mathbf{y}_i)$, and $B_{i,j}$ is the jth strip integral over the ith basis function. Thus, the elements, $A_{i,j}$, of the matrix **A** in (3) are given by

$$A_{i,j} = \frac{1}{\Delta\eta}\Lambda_i B_{i,j}.$$

Note that the matrix $\mathbf{B} = [B_{i,j}]$ is sparse provided that the supports of the basis functions are small, for then each integration strip intersects only a few of them. Naturally, the discretization matrix, **A**, inherits this sparsity, as seen in Fig. 3.

In our implementation the number of basis functions used is dependent on the wavenumber limits, which are constrained by the radar frequency and noise level, and the choice of the parameters controlling the functional representation as mentioned above. For the examples in this paper a typical discretization has 30 centers in angle and 60–80 in wavenumber, so 1800–2400 basis functions are used.

c. Inversion by the row-action method

Large sparse linear systems are common in many applications, and numerous techniques are available for solving them. Systems, such as (3), having an (essentially) unstructured sparsity are an important subclass as they arise in the discretization of tomographic and similar problems. A popular class of solution methods are the *row-action* methods—iterative techniques, where the next iterate $\boldsymbol{\xi}^{(k+1)}$ is found using only the data $\boldsymbol{\xi}^{(k)}$, $\boldsymbol{\sigma}$, and the $i(k)$th row $\mathbf{A}_{i(k)}$ of the matrix **A**, where the sequence $[i(k)]$ cycles through the rows of **A** in some fashion.

The obvious computational advantages of row-action methods have prompted a substantial research effort into their convergence properties, techniques that improve their speed and stability, and so on. We refer the interested reader to Censor's (1981) excellent review.

It is notable that the algorithm of Wyatt for the inversion of the linearized Barrick–Weber equations (Wyatt 1990) has many of the characteristics of a row-action method. The success of Wyatt's algorithm in practical real-time oceanic remote sensing applications (Wyatt et al. 2003) provided the motivation for the discretization described above, and one finds that the natural reimplementation of the iterative step in Wyatt's algorithm produces an *explicit* row-action method. In the remainder of this paper we investigate and optimize this and two other row-action methods for the solution of the linearized Barrick–Weber equations.

1) Algebraic reconstruction technique

The algebraic reconstruction technique (ART) is the oldest of the row-action methods, being proposed as a solution method for the convex feasibility problem by Kaczmarz in 1937. The algorithm was later rediscovered by Gordon et al. (1970) and implemented in the EMI computerized tomography scanner (Hounsfield 1973). For ART the iterative step is

$$\xi_j^{(k+1)} = \xi_j^{(k)} + \lambda \frac{\sigma_{i(k)} - \mathbf{A}_{i(k)} \cdot \boldsymbol{\xi}^{(k)}}{\|\mathbf{A}_{i(k)}\|_2^2} A_{i(k),j} \quad (j = 1, \ldots, n),$$

where $0 < \lambda < 2$ is the *relaxation* parameter. The ART has an attractive geometric interpretation when $\lambda = 1$, for then the iterative step gives the orthogonal projection of $\boldsymbol{\xi}^{(k)}$ onto the hyperplane defined by the $i(k)$th row of the system (3).

A number of theoretical results are available for ART, particularly in the underrelaxed ($0 < \lambda < 1$) case. For example, when applied to a consistent but underdetermined system, underrelaxed ART will converge to the solution of the minimum norm (Censor 1981, section 4.4). It has also been shown (Fleming 1990) that the early termination of the ART iteration is equivalent to Tikhonov regularization, an important consideration when the problem to be discretized is ill-posed, as is the case for the inversion of the x-ray transform.

2) Multiplicative ART

The multiplicative algebraic reconstruction technique (MART) is the row-action method with the iterative step

$$\xi_j^{(k+1)} = \left(\frac{\sigma_{i(k)}}{\mathbf{A}_{i(k)} \cdot \boldsymbol{\xi}^{(k)}} \right)^{\lambda A_{i(k),j}} \xi_j^{(k)} \quad (j = 1, \ldots, n).$$

It can be shown that, if the system $\boldsymbol{\sigma} = \mathbf{A}\boldsymbol{\xi}$ is consistent, then this iteration converges to the solution $\boldsymbol{\xi}$, which minimizes the *entropy*,

$$\sum_j \xi_j \log \xi_j,$$

provided that the elements of $\mathbf{A}$ satisfy $0 \leq A_{i,j} \leq 1$. To ensure that this condition is satisfied, Byrne (2000) recommends a rescaling of the system to obtain the iteration

$$\xi_j^{(k+1)} = \left(\frac{\sigma_{i(k)}}{\mathbf{A}_{i(k)} \cdot \boldsymbol{\xi}^{(k)}} \right)^{\lambda A_{i(k),j}/m} \xi_j^{(k)} \quad (j = 1, \ldots, n),$$

where $m_i = \max \{A_{i,j} : j = 1, \ldots, n\}$. This rescaling is included in our implementation of MART.

3) Chahine–Twomey–Wyatt

Our final algorithm is a reimplementation of that proposed by Wyatt (1990) specifically for the inversion of the linearized Barrick–Weber equations. The original specification of the algorithm included a discretization that has been replaced by that described in section 2b. Wyatt's iteration, a two-dimensional version of that of Chahine (1968) later modified by Twomey (1996), has the iterative step

$$\xi_j^{(k+1)} = \left[1 + \lambda \frac{A_{i(k),j}}{\|\mathbf{A}_{i(k)}\|_\infty} \left(\frac{\sigma_{i(k)}}{\mathbf{A}_{i(k)} \cdot \boldsymbol{\xi}^{(k)}} - 1 \right) \right] \xi_j^{(k)} \quad (j = 1, \ldots, n).$$

Here, $\|\mathbf{A}_i\|_\infty$ is the maximum value of the $A_{i,j}$ for $j = 0, \ldots, n$ and, again, $0 < \lambda \leq 1$ is the relaxation parameter. The motivation for the form of the iteration is detailed by Twomey (1996) who, interestingly, notes his impression that the iteration is particularly suited to the recovery of functions with a large dynamic range—a typical property of ocean wave directional spectra.

3. Synthetic spectra

To investigate the behavior of the iterative schemes in the inversion of the wave spectrum, we have generated synthetic Doppler spectral test data. Note that there is no question of an inverse crime (Colton and Kress 1998, pp. 133, 304) being committed here: our synthesis of Doppler spectra is by a direct discretization of the nonlinear Eq. (2) along the contours defined by the Dirac constraint therein; our inversion uses the radial basis discretization of the linearized equation described in section 2b.

Synthetic Doppler spectra were produced assuming directional ocean spectra with wind waves of the Pier-

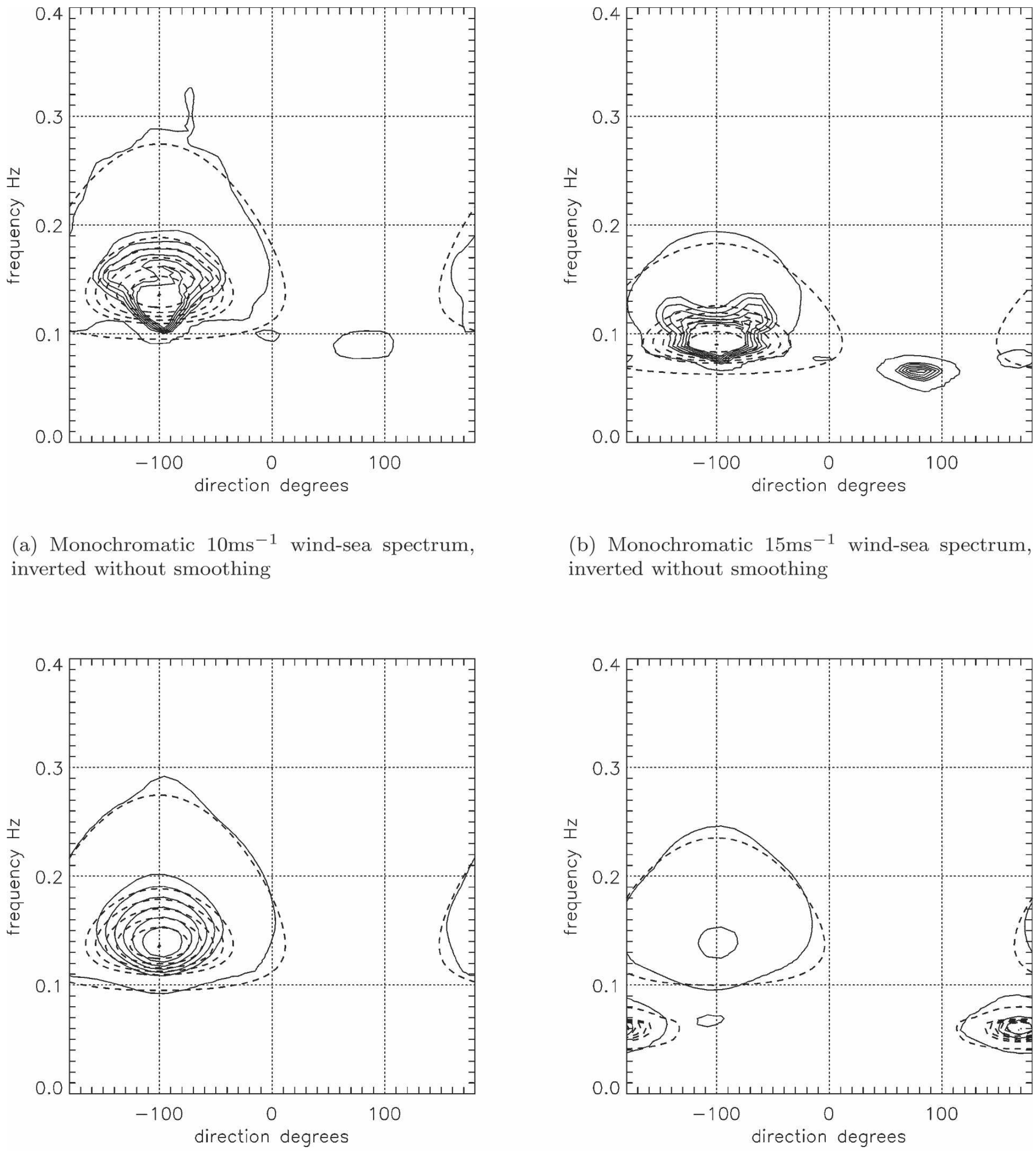

(a) Monochromatic 10ms^{-1} wind-sea spectrum, inverted without smoothing

(b) Monochromatic 15ms^{-1} wind-sea spectrum, inverted without smoothing

(c) As (a), but inverted with smoothing

(d) Bimodal spectrum, with smoothing

FIG. 4. Wave spectra reconstruction.

son–Moskowitz type, in some cases with added swell, and using Barrick–Weber's Eq. (2). Two such Doppler spectra were then inverted using the various methods and these were compared with the original model spectrum. The likeness of the various inversions was broadly similar, but with a definite superiority in recovery for CTW over ART, and for ART over MART.

A typical recovery for CTW with unit relaxation and 200 iterations is shown in Fig. 4, where we note that the inversion has the gross features of the original wave spectrum. However, as can be seen in Figs. 4a and 4b, there is some "splitting" of the spectral peak of the recovered spectrum at lower wave frequencies, and the emergence of spurious modes (this splitting is more pronounced for the ART and MART inversions; not shown). We interpret this as indicating that the smoothing imposed by the discretization alone is not sufficient to regularize the inversion problem. Moreover, there is a limit on how much smoothing can be imposed by our discretization: the radial basis functions must have small support if the approximations underpinning the discretization are to remain valid.

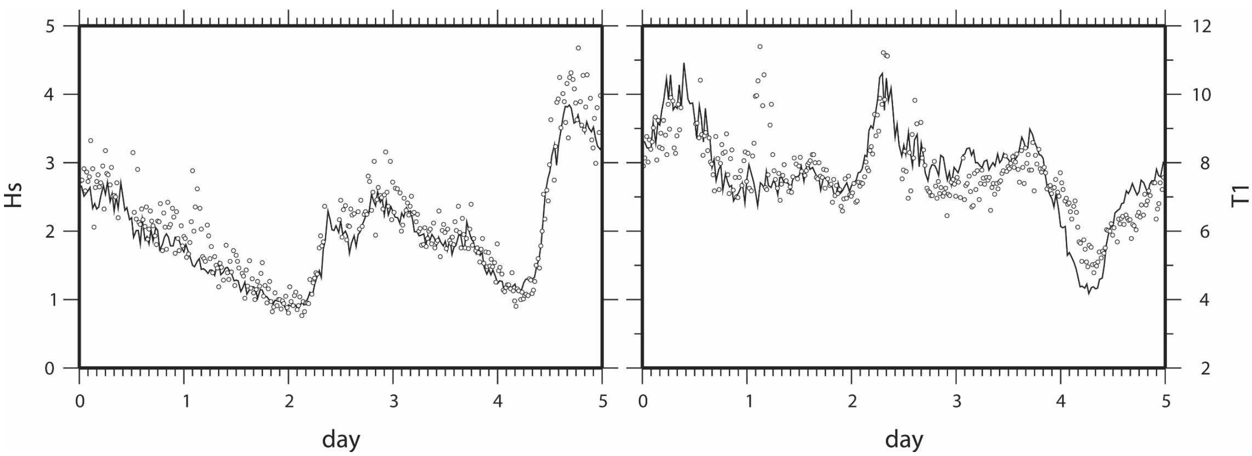

FIG. 5. Parameters for the test period: buoy solid, inversion circles.

Further, the regularizing effects of taking a small relaxation parameter or of the use of a small number of iterations are difficult to exploit here; such inversions have problems recovering swell components of the directional wave spectrum, which typically need scores of iterations to emerge. We would suggest that the underlying problem is that row-action methods not address the anisotropy of the inversion problem.

Our solution is to apply a mild smoothing on candidate solutions between iterative steps, implemented (for simplicity) in a three-point smoothing kernel applied to the representation coefficients in both the wavenumber and direction. We find that good results are obtained if less smoothing is applied to higher frequencies than to lower ones, and so apply it with a kernel of [0.1, 0.8, 0.1] for large wavenumbers decreasing linearly to [0.2, 0.6, 0.2] for small wavenumbers. This seems to provide sufficient regularization to produce inverted wave spectra without peak-splitting, as shown in Fig. 4c. Moreover, this smoothed algorithm is able to distinguish between the different modes in a genuinely bimodal spectrum, as in Fig. 4d.

4. Wave buoy comparison

The European Radar Ocean Sensing (EuroROSE; Wyatt et al. 2003) project was a European Union (EU) funded initiative designed to demonstrate the use of radar sensors for vessel traffic service applications. The Wellen Radar (WERA) HF radar, developed by the University of Hamburg (Gurgel et al. 1999), was deployed in two experiments in 2000. One of these was at the Norwegian coastal islands northwest of Bergen, the site of the Vessel Traffic Service center guiding large oil tankers into mainland ports. The radar was deployed for a period of about 6 weeks providing measurements of the wave and current fields from the coast to up to 40 km offshore with 1-km resolution every 10 min. A microwave X-band radar, a directional wave buoy, an acoustic Doppler current profiler (ADCP), and wave and current models were also used; and the radar and model data were made available in near–real time to the staff in the center.

Detailed comparisons between the wave-measuring instruments and the model are presented in Wyatt et al. (2003). These results confirm previous work (Wyatt et al. 1999) showing an overestimation in HF-radar-measured wave height and an underestimation in wave period in high sea conditions. This is thought to be due to limitations in the scattering model used by Weber and Barrick (1977) and is the subject of current research. For the assessment of the accuracy of the inversion method discussed here we have therefore selected a period of relatively low seas. Since the experiment took place in the winter on an exposed North Atlantic coast and was therefore dominated by storms, the period selected is quite short: 17–21 February 2000, but does include enough variation in wave height and period (see Fig. 5) and also in direction to give us confidence in the generality of our results as far as the numerical methodology is concerned. The comparison presented here is with a directional waverider buoy, which is currently the accepted standard for wave measurements. This buoy provides measurements of five Fourier coefficients of the directional distribution: a_0, a_1, a_2, b_1, and b_2, which are all functions of wave frequency (Tucker 1991). This is thus a more limited measurement than can be obtained with the radar, which provides the full directional spectrum, $S(\mathbf{k})$. Here we will focus on just three integrated parameters that are commonly used to describe the wave field: significant wave height, mean period, and mean direction. We re-

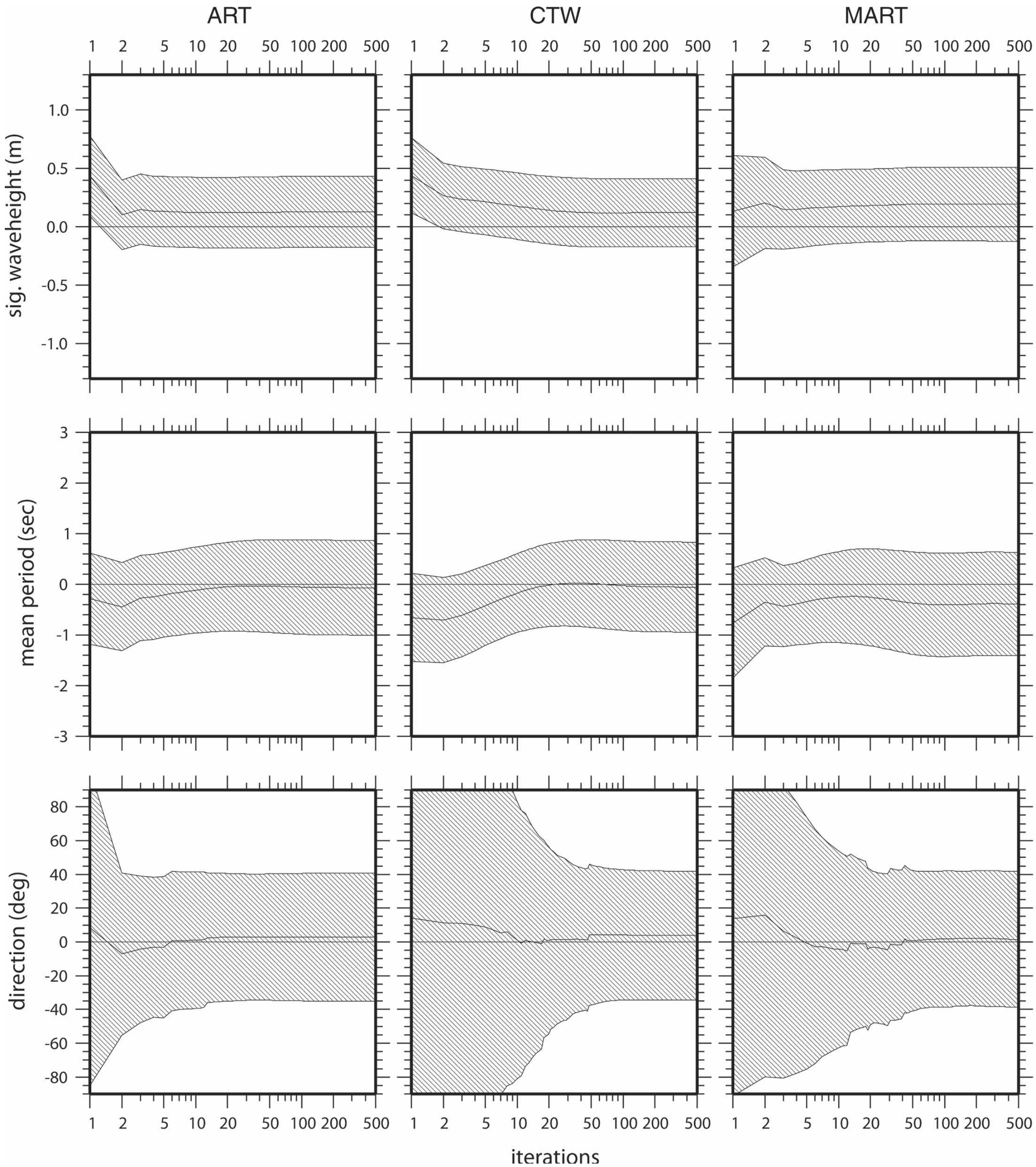

FIG. 6. Mean absolute error between inversion and buoy.

fer the reader to Tucker (1991) for the definitions of and formulas for these quantities.

The data available for the comparison were recorded at different times: inverted spectra every 10 min, buoy data every 30. Consequently, we paired each buoy observation with the nearest inversion (with a maximum difference of 10 min) yielding 334 such pairs in the test period. Summary statistics on the differences between the integrated parameters were then calculated for a range of values of parameters affecting the row-action inversion; the number of iterations and the relaxation parameter λ among them.

Sample results from the comparison for the number of iterations (in the range 1–500) with unit relaxation are illustrated in Fig. 6. As can be seen, each row-action method has rather similar behavior, with the mean difference between buoy and inversion decreasing to a stable value with increasing iterations. The variance in the difference behaves similarly, albeit with more iterations needed to achieve stability, particularly for the differences in mean direction (bottom row of Fig. 6).

Some differences between the row-action methods are apparent from these comparisons: the MART method seems to have a small negative bias in mean period, an effect that is not so pronounced in ART and CTW, and clearly ART outperforms both CTW and MART in the number of inversions needed to achieve convergence to the mean direction value.

The comparisons for various values of the relaxation parameter λ (not shown for reasons of space) for a fixed number of iterations reveal a similar picture, with the differences between buoy and inversion decreasing to a stable value as λ increases from a small value. Indeed, the results suggest that the inversion behaves as if a superposition were occurring: a row-action inversion with n iterations and relaxation of λ is very similar to one with $2n$ iterations and relaxation of $\lambda/2$.

We also mention that the comparisons seem rather insensitive to variations in a number of other details of the row-action method, and even the discretization. There seems to be little effect on the buoy intercomparison when varying the amount of smoothing between iterations (in contrast to the results of section 3, but perhaps not surprising given that we are comparing integrated parameters). We also find that reordering the rows in the discretization matrix prior to inversion (a common strategy for improving the convergence of row-action inversion of problems in transmission tomography) has little effect on the statistics. Finally, we find that varying the number of basis functions used in the discretization has little effect above a certain threshold; this threshold is presumably determined by the breakdown in validity of a number of approximations used in the derivation of the discretization.

5. Ill-posedness

Many problems of mathematical physics can be expressed in the form $y = Ax$, where A is an (possibly nonlinear) operator between function spaces, y is some measured data, and x is to be found. Haddamard considered such problems and declared *well posed* those for which a solution x exists, is unique, and depends continuously on the data y. Ill-posed problems, those which are not well posed, are by no means unphysical; the equation $y = Ax$ is ill-posed whenever the operator A acts to smooth its argument, as is the case for the integral operators arising in the practical problems of metrology, geophysics, and so on. Ill-posedness was, for many years, thought to be mathematically intractable; as late as 1961 Courant was to write, in *Methods of Mathematical Physics II*:

> So far, unfortunately, little mathematical progress has been made in the important task of solving or even identifying such problems which are not "properly posed" but still are important and motivated by realistic situations.

The same decade was to see a revolution in the approach to ill-posedness, that of *regularization*: approximation of an ill-posed problem by a *family* of well-posed problems, each, in a precise sense, near to the original. A. N. Tikhonov, M. M. Lavrentiev, and V. A. Morozov in the East and F. John and S. Twomey in the West reduced the intractability to a problem of a careful choice from the family of approximants.

As has been mentioned earlier in this paper, an expectation that the inversion of the Barrick–Weber equations is ill-posed has been carried into the design of the discretization and the choice of inversion methods, although there are, as far as we know, no analytic results in this direction. In the remainder of this section we present *circumstantial* evidence that the inversion *is* ill-posed, albeit mildly so.

The ill-posedness of the problem $y = Ax$ for linear A is intimately related to the singular value expansion (SVE) of the operator A, as discussed widely in the literature (see, e.g., Hansen 1998, section 1.2.2, chapter 2.2, and Engl et al. 2000, section 2.2). For some problems, for example when A represents the Radon transform, the SVE can be obtained exactly (Natterer and Wübbeling 2001, theorem 2.9). Even when this is not the case we can draw some conclusions from the singular value decomposition (SVD) of the discretization matrix of the problem; the singular values of the operator approximate those of the matrix under mild conditions (Hansen 1998, section 2.1). With this motivation we have found the first 60 singular values of our discretization of the linearized Barrick–Weber equations using the SVDPACK codes (Berry 1992), with the results shown in Fig. 7. A regression on these values gives an estimate of $\sigma_n \sim n^{-1.9}$ and repeating the calculations for a range of 237 locations (and so discretization geometries) as would occur in practical inversion helps us find a decay estimate of $\sigma_n \sim n^{\alpha}$, where α has a mean of -1.88 and a standard deviation of 0.105.

This apparent subquadratic decay of the singular values would suggest that the inversion is, to use the informal classification of Engl et al. (2000, section 2.2), mildly ill-posed and so requires only moderate regular-

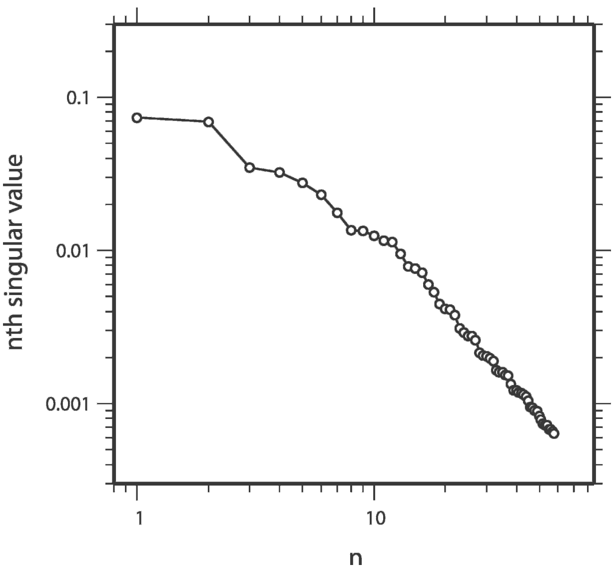

FIG. 7. Singular values.

ization to achieve stability. It is worth noting that the problem limited-angle tomography (inversion of the Radon transform when measured data are available in a restricted set of directions) is found to have exponential decay of the singular values and, so, is severely ill-posed (Natterer and Wübbeling 2001, section 6.2), in marked contrast with the Barrick–Weber inversion (all inversion presented here used exactly two Doppler spectra and so there are four "directions"). A notable difference between the two problems is the highly directional kernel $|\Gamma|^2$ present in the Barrick–Weber equations.

6. Conclusions

Our investigations of the Barrick–Weber problem suggests that the smoothing imposed by our discretization is not sufficient to fully stabilize the inversion by the row-action method. However, the addition of a mild smoothing between row-action iterations does provide this regularization, giving reasonable results in inverting both synthetic and real Doppler spectral data. Consistent with the evidence of mild ill-posedness, we find that all of the row-action methods give similar results but with ART and CTW having a slight advantage over MART in the speed and accuracy of the recovery of integrated parameters. With the added smoothing and unit relaxation, around 50–100 iterations seem sufficient to achieve convergence.

Further research is under way to determine methods whereby the smoothing in the inversion is incorporated more closely into the discretization, so as to give a more fine-grained control over the regularization.

Acknowledgments. The first author was partially supported in this work by the U.K. Natural Environment Research Council (NERC) under Grant NER/A/S/2001/00453.

REFERENCES

Barrick, D. E., and B. L. Weber, 1977: On the nonlinear theory for gravity waves on the ocean's surface. Part II: Interpretation and applications. *J. Phys. Oceanogr.,* **7,** 11–21.

——, and B. J. Lipa, 1986: The second-order shallow-water hydrodynamic coupling coefficient in interpretation of HF radar sea echo. *IEEE J. Oceanic Eng.,* **11,** 310–315.

Berry, M., 1992: Large scale singular value computations. *Int. J. Supercomput. Appl.,* **6,** 13–49.

Byrne, C., 2000: Block-iterative interior point optimization methods for reconstruction from limited data. *Inverse Problems,* **16,** 1405–1419.

Censor, Y., 1981: Row-action methods for huge and sparse systems and their applications. *SIAM Rev.,* **23,** 444–466.

Chahine, M. T., 1968: Determination of the temperature profile in an atmosphere from its outgoing radiance. *J. Opt. Soc. Amer.,* **58,** 1634–1637.

Colton, D., and R. Kress, 1998: *Inverse Acoustic and Electromagnetic Scattering Theory.* 2d ed., Vol. 93, Applied Mathematical Sciences, Springer, 334 pp.

Engl, H. W., M. Hanke, and A. Neubauer, 2000: *Regularization of Inverse Problems*. Vol. 374, Mathematics and Its Applications, Kluwer Academic, 321 pp.

Fleming, H. E., 1990: Equivalence of regularization and truncated iteration in the solution of ill-posed image reconstruction problems. *Linear Algebra Appl.,* **130,** 133–150.

Gordon, R., R. Bender, and G. T. Hermann, 1970: Algebraic reconstruction techniques (ART) for three-dimensional electron microscopy and x-ray photography. *J. Theoret. Biol.,* **29,** 471–481.

Green, J. J., 2002: Approximation with the radial basis functions of Lewitt. *Algorithms for Approximation IV,* J. Leversley, I. Anderson, and J. C. Mason, Eds., University of Huddersfield, 212–219.

——, 2003: Discretising Barrick's equations. *Proceedings of Wind over Waves II: Forecasting and Fundamentals of Applications,* S. G. Sajjadi and J. C. R. Hunt, Eds., IMA and Horwood, 219–232.

Gurgel, K.-W., G. Antonischki, H.-H. Essen, and T. Schlick, 1999: Wellen Radar (WERA): A new ground-wave based HF radar for ocean remote sensing. *Coastal Eng.,* **37,** 219–234.

Hansen, P. C., 1998: *Rank-Deficient and Discrete Ill-Posed Problems. Monographs on Mathematical Modeling and Computation,* Vol. 4, SIAM, 247 pp.

Hounsfield, G. N., 1973: Computerized transverse axial scanning (tomography). I: Description of system. *Brit. J. Radiol.,* **46,** 1016–1022.

Lewitt, R. M., 1990: Multidimensional digital image representations using generalized Kaiser–Bessel window functions. *J. Opt. Soc. Amer.,* **7A,** 1834–1846.

Lipa, B. J., and D. E. Barrick, 1986: Extraction of sea state from HF radar sea echo: Mathematical theory and modeling. *Radio Sci.,* **21,** 81–100.

Natterer, F., and F. Wübbeling, 2001: *Mathematical Methods in Image Reconstruction. Monographs on Mathematical Modeling and Computation*, Vol. 5, SIAM, 216 pp.

Tucker, M. J., 1991: *Waves in Ocean Engineering: Measurement, Analysis, Interpretation.* Ellis Horwood, 431 pp.

Twomey, S., 1996: *Introduction to the Mathematics of Inversion in Remote Sensing and Indirect Measurements.* Dover, 243 pp.

Watson, G. N., 1944: *A Treatise on the Theory of Bessel Functions.* 2d ed. Cambridge University Press, 804 pp.

Weber, B. L., and D. E. Barrick, 1977: On the nonlinear theory for gravity waves on the ocean's surface. Part I: Derivations. *J. Phys. Oceanogr.,* **7,** 3–10.

Wyatt, L. R., 1986: The measurement of the ocean wave directional spectrum from H.F. radar Doppler spectra. *Radio Sci.,* **21,** 473–485.

——, 1990: A relaxation method for integral inversion applied to HF radar measurement of the ocean wave directional spectrum. *Int. J. Remote Sens.,* **11,** 1481–1494.

——, S. P. Thompson, and R. R. Burton, 1999: Evaluation of HF radar wave measurement. *Coastal Eng.,* **37,** 259–282.

——, and Coauthors, 2003: Validation and intercomparisons of wave measurements and models during the EuroROSE experiments. *Coastal Eng.,* **48,** 1–28.